Nanotoxicology

ISSN: 1743-5390 (Print) 1743-5404 (Online) Journal homepage: http://www.tandfonline.com/loi/inan20

Evaluation of the effect of valence state on cerium oxide nanoparticle toxicity following intratracheal instillation in rats

Katherine M. Dunnick, Anna M. Morris, Melissa A. Badding, Mark Barger, Aleksandr B. Stefaniak, Edward M. Sabolsky & Stephen S. Leonard

To cite this article: Katherine M. Dunnick, Anna M. Morris, Melissa A. Badding, Mark Barger, Aleksandr B. Stefaniak, Edward M. Sabolsky & Stephen S. Leonard (2016) Evaluation of the effect of valence state on cerium oxide nanoparticle toxicity following intratracheal instillation in rats, Nanotoxicology, 10:7, 992-1000, DOI: 10.3109/17435390.2016.1157220

To link to this article: http://dx.doi.org/10.3109/17435390.2016.1157220

http://informahealthcare.com/nan
ISSN: 1743-5390 (print), 1743-5404 (electronic)

Nanotoxicology

Nanotoxicology, 2016; 10(7): 992–1000
 DOI: 10.3109/17435390.2016.1157220

Taylor & Francis
Taylor & Francis Group

ORIGINAL ARTICLE

Evaluation of the effect of valence state on cerium oxide nanoparticle toxicity following intratracheal instillation in rats

Katherine M. Dunnick[1,2], Anna M. Morris[1], Melissa A. Badding[1], Mark Barger[1], Aleksandr B. Stefaniak[3], Edward M. Sabolsky[4], and Stephen S. Leonard[1,2]

[1]HELD, National Institute for Occupational Safety and Health, Morgantown, WV, USA, [2]Pharmaceutical and Pharmacological Sciences, West Virginia University, Morgantown, WV, USA, [3]RHD, National Institute for Occupational Safety and Health, Morgantown, WV, USA, and [4]WVU Benjamin M. Statler College of Engineering and Mineral Resources, Morgantown, WV, USA

Abstract

Cerium (Ce) is becoming a popular metal for use in electrochemical applications. When in the form of cerium oxide (CeO_2), Ce can exist in both 3 + and 4 + valence states, acting as an ideal catalyst. Previous *in vitro* and *in vivo* evidence have demonstrated that CeO_2 has either anti- or pro-oxidant properties, possibly due to the ability of the nanoparticles to transition between valence states. Therefore, we chose to chemically modify the nanoparticles to shift the valence state toward 3+. During the hydrothermal synthesis process, 10 mol% gadolinium (Gd) and 20 mol% Gd, were substituted into the lattice of the CeO_2 nanoparticles forming a perfect solid solution with various A-site valence states. These two Gd-doped CeO_2 nanoparticles were compared to pure CeO_2 nanoparticles. Preliminary characteristics indicated that doping results in minimal size and zeta potential changes but alters valence state. Following characterization, male Sprague-Dawley rats were exposed to 0.5 or 1.0 mg/kg nanoparticles via a single intratracheal instillation. Animals were sacrificed and bronchoalveolar lavage fluid and various tissues were collected to determine the effect of valence state and oxygen vacancies on toxicity 1-, 7-, or 84-day post-exposure. Results indicate that damage, as measured by elevations in lactate dehydrogenase, occurred within 1-day post-exposure and was sustained 7-day post-exposure, but subsided to control levels 84-day post-exposure. Furthermore, no inflammatory signaling or lipid peroxidation occurred following exposure with any of the nanoparticles. Our results implicate that valence state has a minimal effect on CeO_2 nanoparticle toxicity *in vivo*.

Keywords

Cerium oxide, intratracheal instillation, nanoparticles, nanotoxicity, valence state

History

Received 7 December 2015
Revised 18 February 2016
Accepted 18 February 2016
Published online 10 March 2016

Introduction

Ce, the most abundant rare earth metal and a member of the lanthanide series, has been implicated in Ce pneumoconiosis, a restrictive lung disease characterized by severe pulmonary fibrosis and emphysema (Pairon et al., 1995; Vocaturo et al., 1983). Ce-containing rare earth metal dusts, which are used in industry for glass polishing and photoengraving, have also been associated with severe pulmonary fibrosis and extensive Ce particle accumulation in the lungs of industry workers (Pairon et al., 1994). One study presented data that Ce can remain within workers' lungs for more than 20 years (Pairon et al., 1994). Thus, the production of new materials containing Ce, such as cerium oxide (CeO_2) nanoparticles, necessitates toxicity studies to evaluate potential worker exposure risks. To date, the literature on CeO_2 nanoparticle toxicity is conflicted. Due to the variety of uses for CeO_2 nanoparticles, including use in electrochemical sensors, fuel cells, and reforming catalysts as well as use as a diesel fuel additive to reduce emissions and increase engine efficiency (Cassee et al., 2011), toxicity screenings of this nanomaterial and determination of CeO_2 pulmonary effects is essential.

Correspondence: Katherine Dunnick, HELD, National Institute for Occupational Safety and Health, PPRB, 1095 Willowdale Rd, Morgantown, WV 26505, USA. E-mail: kdunnick@mix.wvu.edu

Previous *in vitro* studies of the toxicity of CeO_2 nanoparticles have shown conflicting toxicity results. For example, studies completed in immune cells have reported that CeO_2 protects against induced apoptosis in human lymphocytes (Celardo et al., 2011) or acts as an antioxidant under conditions of induced oxidative stress in mouse monocyte macrophage cells (Xia et al., 2008). Further, studies conducted in colon cells showed CeO_2 nanoparticles were capable of preventing radiation-induced damage through antioxidant-like properties (Colon et al., 2010). Conversely, studies in various epithelial cell lines indicated that CeO_2 either exerts toxicity through reactive oxygen species (ROS) production (Eom & Choi, 2009; Lin et al., 2006; Park et al., 2008) or elicits only mild ROS and has antioxidant-like properties (Xia et al., 2008). These results imply that CeO_2 toxicity varies between cell type and within similar cell types.

The conflicting *in vitro* data are theorized to be a result of the ability of Ce to readily transition between 3+ and 4+ valence states (Das et al., 2007). When Ce is in the 3+ valence state, it is hypothesized that it exerts antioxidant potential, while in the 4+ valence state it produces free radicals and causes oxidative damage (Celardo et al., 2011; Das et al., 2007; Park et al., 2008). To assess the importance of valence state and concentration of oxygen vacancies within the material in influencing CeO_2 reactivity and toxicity, a technique known as doping was employed to modulate the electrical properties of the nanoparticles and force them toward a greater 3+/4+ ratio by incorporating

gadolinium (III) oxide (Gd_2O_3) into the nanoparticles (Wang et al., 2011). Two different samples of CeO_2 nanoparticles were doped and used in this study: a 10 mol% and 20 mol% Gd in CeO_2. Pure, unaltered CeO_2 nanoparticles were also tested in addition to a Gd_2O_3 nanoparticle control to ensure any effects seen between compounds were due to valence state and oxygen vacancies rather than the presence of Gd_2O_3, which is known to induce acute lung toxicity (Yoneda et al., 1995). Initial *in vitro* tests by our group determined that as particle doping increased, the antioxidant potential of CeO_2 nanoparticles decreased in both RLE-6TN alveolar epithelial and NR8383 alveolar macrophage rat cells (Dunnick et al., 2015). Others have also shown that valence state had no effect on *in vitro* toxicity, but as the 3+/4+ ratio decreased, the antioxidant potential of the nanoparticles also decreased (Celardo et al., 2011).

In vivo studies have shown that CeO_2 nanoparticles cause substantial pulmonary damage, induce inflammation, and induce fibrosis at a range of doses using a variety of exposure methods, including intratracheal (IT) instillation and inhalation (Demokritou et al., 2013; Ma et al., 2012). Ma et al. (2011) have shown that at doses ranging from 0.15 mg/kg to 7 mg/kg, rats presented with markers of fibrosis within 28-day post-IT exposure. A study in which rats were exposed to CeO_2 nanoparticles via mouth/nose inhalation showed similar toxicity results and inflammatory cytokine activation, but also demonstrated significant increases in ROS production and disruptions in antioxidant systems (Srinivas et al., 2011). Aalapati et al. (2014) also presented data that following inhalation studies in mice, CeO_2 nanoparticles induced oxidative stress as measured by induction of lipid peroxidation (LPO) and decreased glutathione. This change in ROS was not detected in comparable *in vivo* studies (Demokritou et al., 2013). In addition, studies have also shown that surface coatings influence the relative toxicity of CeO_2 nanoparticles. For example, when CeO_2 nanoparticles were coated with amorphous silica, researchers recorded decreased CeO_2 induced inflammation and fibrosis (Ma et al., 2015). Thus, it may be possible that alterations of the physical properties of the CeO_2 nanoparticles may decrease their relative reactivity and overall toxicity.

While previous studies have been conducted to determine the toxicity of CeO_2 nanoparticles following deposition in the lungs of rats, this is the first study to assess *in vivo* changes in reactivity and toxicity following chemical alteration to the nanoparticles in a way that affects valence state. The aim of this study was to determine the effect of valence state and oxygen vacancies on CeO_2 reactivity *in vivo* in order to possibly explain discrepancies among studies while addressing the possible cause for these differences. To accomplish this, Sprague-Dawley rats were exposed intratracheally to pure CeO_2, CeO_2 with 10 mol% Gd, or CeO_2 with 20 mol% Gd nanoparticles. Rats were sacrificed 1-, 7-, or 84-day post-one time nanoparticle exposure and overall pulmonary toxicity, ROS, inflammation, and pulmonary changes were assessed to address the hypothesis that valence state affects CeO_2 *in vivo* toxicity.

Materials and methods

CeO_2 nanoparticle production and characterization

Gd-doped CeO_2 nanopowder was prepared as previously described (Dunnick et al., 2015). Briefly, a hydrothermal method was used in which cerium (IV) ammonium nitrate and gadolinium nitrate hexa-hydrate were dissolved in deionized water and mixed together. Tetramethyl ammonium hydroxide was added to the mixture until the pH reached 10, followed by precipitate formation. The precipitate was washed and hydrothermally treated at 240 °C for 1 h to obtain the final nanoparticles.

X-ray photoelectron spectroscopy (XPS) was utilized to determine the changes in valence state between samples as previously described (Dunnick et al., 2015). To determine the relative size of the nanoparticles in phosphate-buffered saline (PBS), dynamic light scattering (DLS) was performed using a Nano ZS90 instrument (Malvern Instruments, Worcestershire, UK). Prior to sample measurement, sample cells were cleaned, rinsed, and pre-wetted with filtered PBS. Samples were exposed to ultrasonic agitation for 10 min using a probe tip to produce a uniform dispersion.

To determine the relative dispersion stability of the nanomaterials, zeta potential of CeO_2, and Gd-doped CeO_2 nanoparticles in PBS were performed using a Nano ZS90 instrument (Malvern Instruments). The viscosity of the PBS was determined at room temperature using a VS-10 viscometer (Malvern Instruments) for use in determining zeta potential. Each nanoparticle suspension was sonicated for 10 min using a probe tip to produce a uniform dispersion. The Smoluchowski approximation of 1.5 was used for Henry's function and a pH of 7.5 was determined for the PBS.

Animal exposures

Male Sprague-Dawley (Hla: SD-CVF) rats (6 weeks old) were purchased from Hilltop Laboratories (Scottdale, PA) and pair housed in an animal facility accredited by the American Association for Assessment and Accreditation of Laboratory Animal Care in pairs in cages individually ventilated cages with HEPA-filtered air. All animals were exposed and euthanized according to a National Occupational Institute for Occupational Safety and Health approved protocol that complied with the Guidelines for the Care and Use of Laboratory Animals. Following a one-week acclimation period, rats were anesthetized with 40 mg/kg sodium methohexital (Brevital, Eli Lily and Co., Indianapolis IN), weighed, and placed on an inclined restraint board. All CeO_2 nanoparticle samples were exposed to ultrasonic agitation for 5 min prior to animal exposure. Nanoparticles were administered via IT at a final concentration of 0.5 mg/kg BW or 1.0 mg/kg BW. PBS was used as a negative control. A minimum of 6 rats were treated per group, for each time point and dose, and sacrificed at 1-, 7-, or 84-day post-exposure. Since CeO_2 nanoparticle exposure does not have a set permissible exposure limit (PEL), animal dosages were selected based on previous studies (Ma et al., 2012).

Bronchoalveolar lavage

At 1-, 7-, and 84-day post-exposure, bronchoalveolar lavage (BAL) was performed on the entire lung to assess lung injury and inflammation ($n = 6$–7/treatment group). Animals were euthanized with sodium pentobarbital (>100 mg/kg) and exsanguinated by cutting the abdominal aorta. The lungs were lavaged with 6 ml Ca^{2+}, Mg^{2+}-free PBS, pH 7.4 to collect the first lavage, followed by 8 ml aliquots of PBS until 40 ml were collected for the second lavage. Lavage fluid centrifuged at $3000 \times g$ for 10 min at 4 °C. Cell-free supernatants from the first lavage were collected for lactate dehydrogenase (LDH) and cytokine analysis. Cell pellets were then re-suspended in 1 ml PBS and evaluated as described below. The first lavage was used for all cellular experiments except chemiluminescence (CL) and electron paramagnetic resonance (EPR) studies, in which cells collected in the second lavage were used.

Cellular evaluation and lactate dehydrogenase measurement

Total cell numbers were determined using a Beckman Coulter Multisizer 4 Analyzer (Beckman Coulter, Indianapolis, IN).

Polymorphonuclear leukocytes (PMN) and alveolar macrophages (AM) counts were also determined. Cells were differentiated using a Cytospin 4 centrifuge (Shandon Life Sciences International, Cheshire, England). Briefly, cell suspensions (2×10^5) were spun for 5 min at $72 \times g$ and pelleted onto a slide. Two hundred cells/rat were then counted following staining with modified Wright-Giemsa stain and the relative abundance of lung AMs, PMNs, lymphocytes, and eosinophils were determined.

Acellular LDH activity from BAL was measured to determine general cell damage and toxicity using a COBAS C111 analyzer (Roche Diagnostic Systems, Montclair, NJ).

Chemiluminescence and electron paramagnetic resonance

Luminol-dependent CL was completed to measure macrophage activity and was monitored using a Berthold LB953 Luminometer (Berthold, Wildbad, Germany). BAL cell (1×10^6 AM/ml) luminescence was measured before and after zymosan stimulation (2 mg/ml; Sigma Chemical Company, St Louis, MO). Zymosan was used for its ability to stimulate and be readily engulfed by activated phagocytic cells (Gantner et al., 2003). Results are presented as zymosan-stimulated minus unstimulated cell CL production.

A 5,5′-dimethylpryrroline N-oxide (DMPO) spin trap technique was implemented to form long-lived free radicals that could be detected via EPR to assess the reactivity of the cells. EPR measurements were collected using a flat cell assembly and Bruker EMX spectrometer (Billerica, MA). Second BAL cells (1×10^6 AM/ml) were combined with 200 mM DMPO (Sigma Aldrich), and 2 mM Cr (VI) for 3 min at 37 °C prior to hydroxyl radical measurement. Instrument settings are indicated in the figure legend. Signal intensity (peak height) was used to measure the relative amount of superoxide radicals produced and is measured in millimeters. All data are presented as peak height fold change above control animal AM response to Cr (VI).

Table 1. Nanoparticle characteristics in PBS.

Nanoparticle	Hydrodynamicdiameter (nm)	Zeta potential
CeO_2	1166 ± 74	−32.1 ± 3.0
CeO_2 10% Gd	2078 ± 32	−26.9 ± 4.1
CeO_2 20% Gd	2436 ± 56	−23.4 ± 1.8

Lipid peroxidation measurements

Following lavage, a segment of the right lung was removed from each animal and immediately placed in −80 °C. LPO values, specifically malondialdehyde (MDA) levels, were determined according to the manufacturer's protocol (OxisResearch, Beverly Hills, CA) and samples were run in duplicate. Lung tissue was combined with ice-cold PBS (100 mg/ml) and butylated hydroxytoluene (50 mM) and homogenized for 30 s. Following homogenization, samples were centrifuged at $2500 \times g$ for 10 min at 4 °C. Two hundred microliters of clear supernatant was removed and placed in a clean glass tube. After addition of kit-specific reagents and incubation at 45 °C for 1 h, samples were centrifuged at $2500 \times g$ for 10 min at room temperature and a clear supernatant was collected and transferred to a glass plate. Absorbance was measured at 586 nm.

Protein analysis

Production of the cytokines TNF-α, IL-8, and IL-6 were determined from first lavage BAL using enzyme-linked immunosorbent assays (ELISAs) according to the manufacturers protocol (Life Technologies, Grand Island, NY) and samples were run in duplicate.

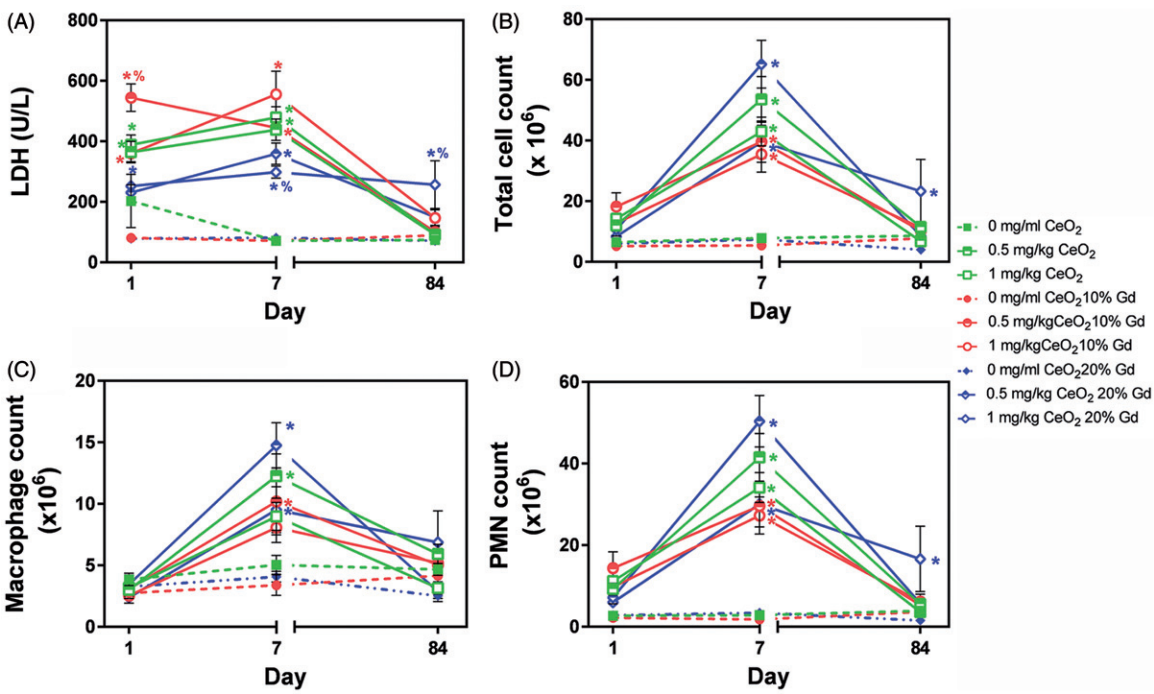

Figure 1. Lactate dehydrogenase (LDH) levels and inflammatory cell counts in rat BAL over a time course of 84-day post-IT exposure. (A) LDH concentration in BAL 1-,7-, and 84-day post-CeO_2 nanoparticle exposure. Square (CeO_2), circle (CeO_2 10% Gd), diamond (CeO_2 20% Gd) symbols represent mean ± SEM ($n = 6$–7 rats/group). 0 mg/kg vehicle control animals are represented by hashed lines. *$p < 0.05$ compared to 0 mg/kg controls on corresponding day, %, $p < 0.05$ compared to pureCeO_2 on corresponding day. Data are represented as mean number of cells and the symbols represent the mean number ± SEM ($n = 6$–7 rats/group). (B) Total cells, (C) macrophages, (D) and PMNs in BAL. *$p < 0.05$ compared to 0 mg/kg controls on corresponding day, %, $p < 0.05$ compared to pure CeO_2 on corresponding day.

Histopathological examination

Histopathological examination was performed on lung liver, and kidney sections from a separate group of 84-day post-CeO_2 nanoparticle or PBS exposed animals, not previously lavaged, using hematoxylin–eosin (H&E) staining on formalin-fixed tissues. Lungs were fixed via tracheal intubation. Following fixation of tissues in 10% buffered formalin, tissues were embedded in paraffin wax, sectioned at 5 µm, mounted on glass slides, and stained. Sections were examined by light microscopy by a board-certified pathologist.

Statistical analysis

Data are represented as the mean ± standard error of the mean (SEM) for each condition. To compare responses, one-way and two-way analysis of variance (ANOVA) and Tukey post-test were performed using GraphPad Prism 6 software (GraphPad Software Inc., La Jolla, CA). Statistical significance is shown between treatment groups when $p < 0.05$.

Results

CeO_2 nanoparticle characteristics

To determine the relative size of the nanoparticles in PBS, DLS was utilized and showed that all of the nanoparticles agglomerated into micron-sized particles (Table 1). Data indicate that pure CeO_2 nanoparticles agglomerate less than both doped samples (1166 nm pure CeO_2 vs. 2078 nm CeO_2 10% Gd vs. 2436 nm CeO_2 20% Gd). All nanoparticles had a similar spherical morphology. Previous transmission electron microscopy data

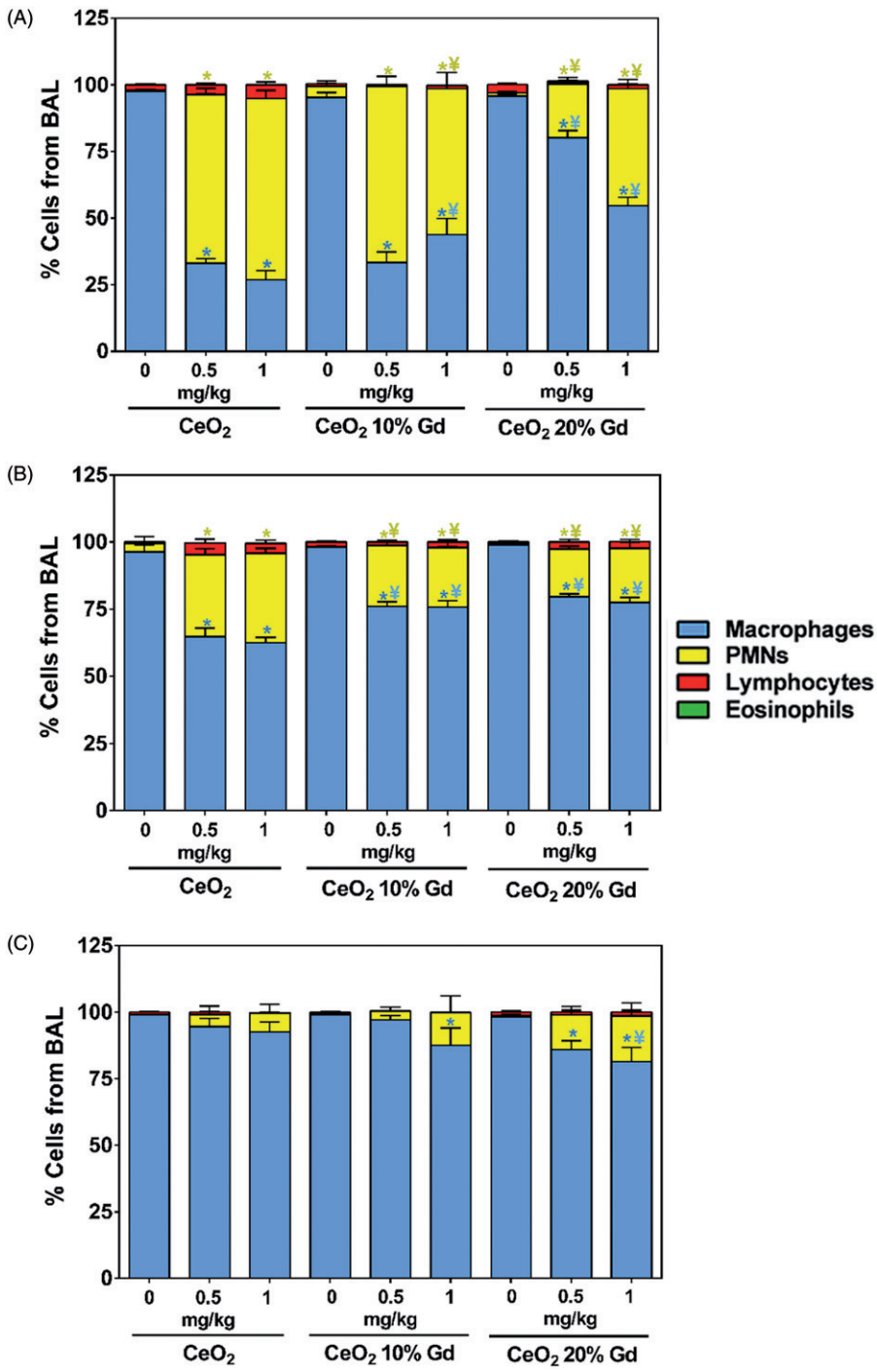

Figure 2. Cell differentials from BAL over a time course of 84-day post-IT exposure. (A) Cells (200/rat) from 1-day post-exposure. (B) 7-day post-exposure. (C) 84-day post-exposure. Data are presented as percentage of cells and the bars represent the mean percentage ± SEM ($n = 6$–7 rats/group). *$p < 0.05$ compared to 0 mg/kg controls on corresponding day, ¥$p < 0.05$ compared to pure CeO_2 on corresponding day.

showed that these particles were approximately 5 nm as-prepared prior to suspension (Dunnick et al., 2015), but quickly agglomerate due to their high surface energy. Zeta potential results also show a similar trend between the nanoparticle samples, as the values fall within the Riddick category of delicate dispersion (Riddick, 1968).

Effect of CeO_2 nanoparticles on pulmonary toxicity and BAL cells

A number of parameters were evaluated from BAL samples to determine the relative toxicity of the nanoparticles. LDH levels were measured to determine the general toxic effects of CeO_2 nanoparticle exposure. LDH data show that cell membrane damage peaked at 7-day post-exposure and returned to baseline LDH levels by 84 days following exposure to CeO_2 and CeO2 10% Gd. However, CeO_2 20% Gd exposure resulted in persistently elevated LDH levels compared to vehicle control animals 84-day post-exposure (Figure 1A). By 7-day post-nanoparticle exposure, total cells counted in BAL were elevated with all nanoparticle exposure groups compared to vehicle control animals (Figure 1B). This significant increase was also reflected in PMN counts. Conversely, only the 0.5 mg/kg dose of CeO_2 and CeO_2 10% Gd and both doses of CeO_2 20% Gd induced significant macrophage influx in BAL (Figure 1C). By 84-day post-exposure, all cell counts returned to normal compared to vehicle control animals with the exception of the high dose of CeO_2 20% Gd, which remained elevated (Figure 1B and D).

Cell differentials showed a similar change in pulmonary cellular composition followed by recovery over the 84-day experiment. BAL composition changed from mainly macrophages in control animals to greater than 50% PMNs following exposure to both pure CeO_2 nanoparticles and CeO_2 10% Gd at both doses 1-day post-exposure (Figure 2A). CeO_2 20% Gd exposure also significantly altered the ratio of macrophages to PMNs relative to PBS control-treated animals. However, the effect was less severe at this time-point compared to pure CeO_2 and CeO_2 10% Gd exposed animals. Pure CeO_2 nanoparticles had a significantly more pronounced effect on cellular composition, specifically increasing PMN and macrophage percentage, compared to both CeO_2 10% Gd and CeO_2 20% Gd 7-day post-IT (Figure 2B). By 84-day post-exposure, BAL cellular composition returned to normal in animals exposed to pure CeO_2, while CeO_2 20% Gd had a persistent effect on cellular composition at both doses (Figure 2C).

Further, an additional set of animals were exposed to Gd_2O_3 nanoparticles alone to ensure any effects measured were due to valence state or transitional ability, rather than the presence of Gd in the doped nanoparticle samples. Gd_2O_3, at a dose equivalent to the amount of Gd present in the CeO_2 20% Gd sample (179 μg/kg), did not have significant effects on LDH or BAL cells by 84-day post-exposure (data not shown). Therefore, the effects caused by CeO_2 20% Gd are potentially due to differences in surface reactivity, valence state, and oxygen vacancies, rather than the presence of Gd.

CeO_2 nanoparticle effects on phagocyte activity

To determine cellular activity, a CL assay was utilized to measure ROS production. At 1-day post-exposure, BAL cells from all nanoparticle-treated rats at both doses significantly responded to zymosan stimulation compared to cells from vehicle control treated rats. Over time, zymosan-treated cells from exposed rats had reduced ROS production, and by 84-day post-exposure, ROS production was further reduced to control levels in all treatment groups (Figure 3A).

To determine phagocyte responsiveness and ROS production, EPR was utilized on recovered BAL cells. In the absence of Cr (VI) stimulus, phagocytic cells did not produce hydroxyl radicals (data not shown). However, following treatment with Cr (VI), phagocytic cells from CeO_2 1 mg/kg at 7-day post-exposure produced significant levels of hydroxyl radicals compared to BAL

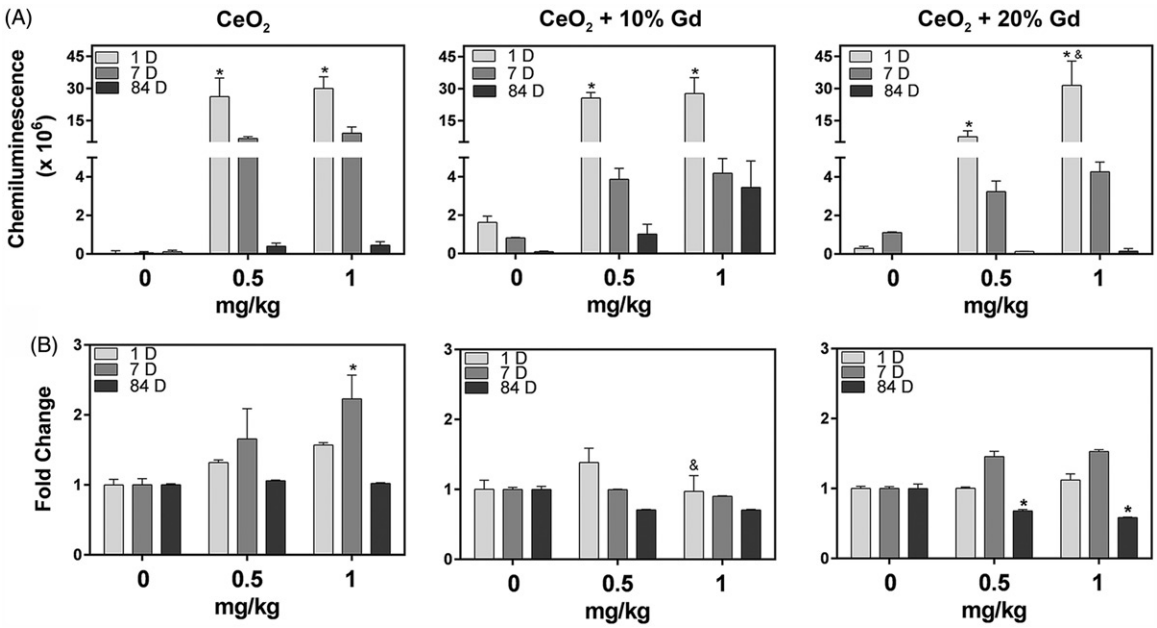

Figure 3. Pulmonary phagocytic cell activity over a time course of 84-day post-exposure. (A) Response of AM from BAL over 84-day post-exposure to zymosan challenge. ROS production was measured via chemiluminescence. $^{*}p < 0.05$ compared to 0 mg/kg controls on corresponding day, $^{\&}p < 0.05$ compared to 0.5 mg/kg dose of same nanoparticle on corresponding day. Data are represented as average luminescence and the bars represent the average ± SEM ($n = 6$–7 rats/group). (B) Phagocytic cell response to Cr (VI) challenge as measured by free radical production via EPR. BAL cells were combined with 200 mM DMPO, and 2 mM Cr (VI) for 3 min. Data represent fold change compared to 0 mg/kg animals and the bars represent the mean ± SEM ($n = 6$–7 rats/group). EPR settings were: center field, 3485 G; scan width, 100 G; time constant, 0.41s; modulation amplitude, 1 G; receiver gain, 1×10^4; frequency, 9.8 GHz; and power, 126.9 mW.

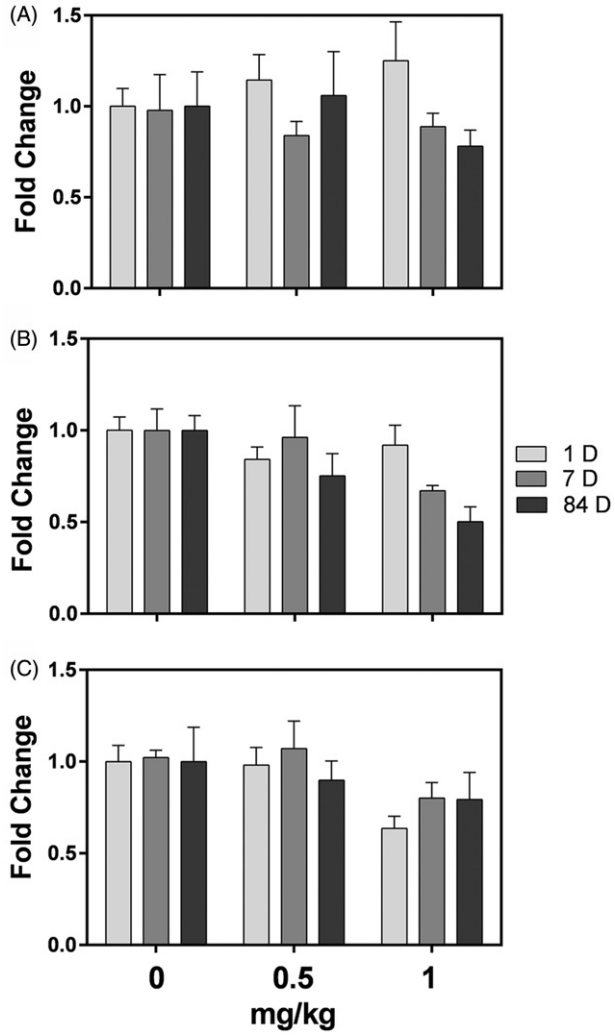

Figure 4. Lipid peroxidation (LPO) in pulmonary homogenates measured as MDA in lung homogenates at 1-, 7-, and 84-day after exposure. Data are represented as fold change compared to 0 mg/kg animals and the bars represent the mean ± SEM ($n = 6$–7 rats/group). (A) CeO_2. (B) CeO_2 10% Gd. C. CeO_2 20% Gd.

cells from vehicle control-treated animals. CeO_2 20% Gd significantly reduced the ability of the phagocytic cells to respond to Cr (VI) 84-day post-exposure (Figure 3B).

CeO_2 nanoparticle exposure does not result in lipid peroxidation or cytokine release within rat lungs

CeO_2 nanoparticles have previously been reported to induce inflammation and affect free radical production (Ma et al., 2011; Srinivas et al., 2011), and therefore, LPO end products and pro-inflammatory markers were examined. To determine downstream damage from free radical generation following nanoparticle exposure, MDA levels were measured in pulmonary homogenates. None of the nanoparticles induced significant LPO at any of the time points (Figure 4). Further, IL-6, TNF-α, and IL-1β, which were measured to determine the pro-inflammatory potential of CeO_2 nanoparticles, were not significantly elevated in BAL by exposure to any of the nanoparticles when compared to vehicle control animals (Figure 5).

CeO_2 nanoparticle histopathological effects

To determine the effect of CeO_2 on alveolar macrophage and granular material accumulation in airways, H&E staining was utilized in lung sections from animals exposed to CeO_2 nanoparticles 84-day post-exposure. All three CeO_2 nanomaterials caused macrophage (multifocal and diffuse) accumulation in the airways and mononuclear cell infiltration in the alveolar septae at both 0.5 mg/kg and 1 mg/kg doses compared to PBS treated animals. Lung lesion severity was generally greater in CeO_2 20% Gd exposed animals (Supplementary Figure 1, Table 2); however, there was no consistent difference in the incidence or severity of lung changes among the animals, making determination of the impact of valence state on pulmonary toxicity difficult to interpret. No significant differences were noted between groups at equivalent doses but there was greater severity of lung lesions in animals exposed to 1 mg/kg compared to those exposed at 0.5 mg/kg. All tissues from the PBS control group were considered within normal limits (Supplementary Figure 1, Table 2). Further, Gd_2O_3 nanoparticle exposed lungs were also considered within normal limits (data not shown). To determine the potential for CeO_2 nanomaterials to cause damage in other organs, kidney and liver sections were stained with H&E. No significant changes in liver or kidney were noted in nanoparticle exposed animals compared to PBS exposed animals (data not shown).

Discussion

As interest in CeO_2 nanoparticles for industrial use increases, worker exposures will likely occur. The purpose of this study was to determine if altering the valence state of Ce within CeO_2 nanoparticles by doping with Gd_2O_3 could mitigate its pulmonary toxicity. Specifically, this study assessed how changes in valence state might affect cellular influx, damage, and inflammation, in the lungs of rats.

As previously shown, doping substantially altered the Ce^{3+}/Ce^{4+} ratio from 16% in the pure CeO_2 nanoparticles to 42% in the 10 mol% doped and to 44% in the 20 mol% doped (Dunnick et al., 2015). Doping did not affect the primary particle size but did affect agglomeration tendencies as increased doping was associated with increased particle agglomeration (Table 1). While doping significantly altered the valence state and oxygen vacancies between the pure and doped samples, this alteration did not dramatically affect the pulmonary toxicity and reactivity of CeO_2 nanoparticles following IT exposures. The overall effect of doping on CeO_2 toxicity is unclear, but it did appear that exposure to CeO_2 20% Gd caused persistent changes (out to 84-day post-IT) in pulmonary cell counts and damage compared to vehicle control animals. Animals exposed to pure CeO_2 or CeO_2 10% Gd nanoparticles did not demonstrate significant increases in these parameters by the end of the study (Figure 2C). The difference in reactivity between the two doped samples was surprising due to minimal differences in Ce^{3+}/Ce^{4+} ratio between the doped nanoparticle samples. However, based on our previous *in vitro* studies, valence state may be less important in modulating CeO_2 nanoparticle reactivity (Dunnick et al., 2015). However, the content of oxygen vacancies is higher in the CeO_2 20% Gd, indicating that differences in pulmonary toxicity may be due to changes in the redox potential of the nanomaterials. Therefore, the process of doping may limit the ability of nanoparticles to switch between valence states and increase oxygen vacancies, which may affect their reactivity in the pulmonary environment. A study conducted in mice also found that the pulmonary response to nanoparticle exposure was affected by the redox activity of CeO_2 nanoparticles (Peng et al., 2014). Data from Peng et al. (2014) indicated that CeO_2 nanoparticles with increased redox activity, as measured by glutathione, glutathione peroxidase, and catalase levels in lung homogenates, induced a mild initial pulmonary response but had more persistent long term effects compared to less redox active particles.

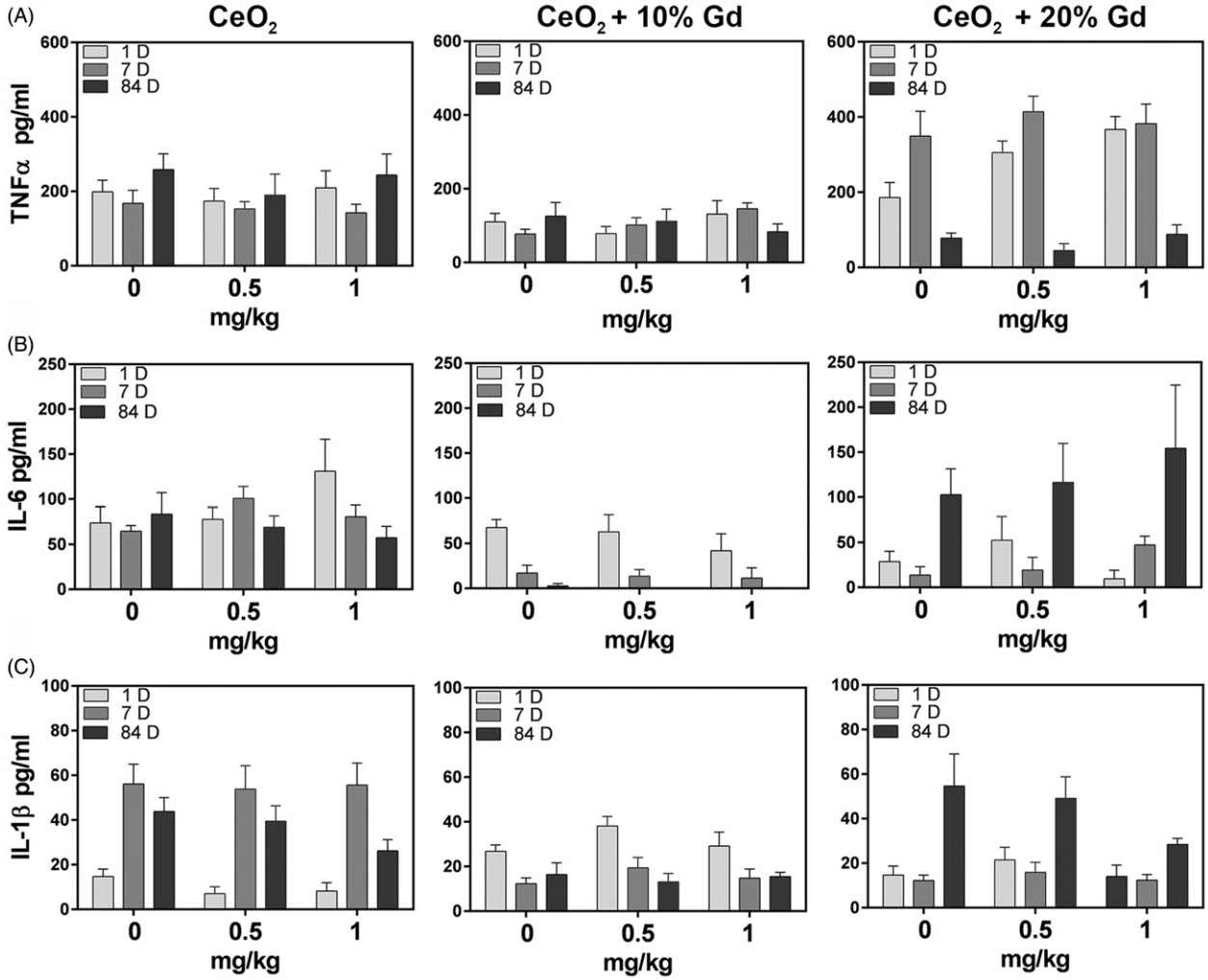

Figure 5. Cytokine concentration in BAL over a time course of 84-day post-exposure. A Concentrations of (A) TNF-α, (B) IL-6, or (C) IL-1β in BAL from nanoparticle-treated rats were quantified.

Table 2. Histopathological findings 84-day post-IT exposure to nanoparticles.

	Particle type						
	PBS	CeO_2		CeO_2 + 10% Gd		CeO_2 + 20% Gd	
Histopathology diagnosis	0 mg/kg ($n=5$)	0.5 mg/kg ($n=6$)	1 mg/kg ($n=7$)	0.5 mg/kg ($n=6$)	1 mg/kg ($n=6$)	0.5 mg/kg ($n=6$)	1 mg/kg ($n=6$)
Alveolar macrophage accumulation							
Histopathology score	0 ± 0	0.9 ± 0.6	1 ± 1.3	1 ± 0.6	1.3 ± 1.1	0.7 ± 0.7	2.3 ± 0.7
Incidence	0/5	5/6	3/7	5/6	4/6	3/6	6/6
Increased alveolar macrophages							
Histopathology score	0.1 ± 0.3	0.4 ± 0.7	1.6 ± 0.9	1 ± 0	1.2 ± 0.7	1.2 ± 0.7	2 ± 0.6
Incidence	1/5	2/6	6/7	6/.6	5/6	5/6	6/6
Granular material accumulation, alveolar/airway lumens							
Histopathology score	0 ± 0	0.8 ± 0.9	0.9 ± 1.5	0.3 ± 0.7	1 ± 1.2	0.2 ± 0.4	1.3 ± 1.4
Incidence	0/5	1/6	2/7	1/6	3/6	1/6	5/6
Mononuclear cell infiltration, alveolar septae							
Histopathology score	0 ± 0	0.6 ± 0.9	1.8 ± 1.5	0.5 ± 0.8	0.8 ± 0.9	0.7 ± 0.7	1 ± 1
Incidence	0/5	2/6	5/7	2/6	3/6	3/6	4/6
Alveolar septae thickening							
Histopathology score	0.1 ± 0.3	0.7 ± 0.9	2 ± 1.5	0.5 ± 0.8	0.8 ± 0.9	0.7 ± 0.7	1.5 ± 0.8
Incidence	0/5	3/6	5/7	2/6	3/6	3/6	6/6
Hemorrhage							
Histopathology score	0.4 ± 0.5	0.6 ± 0.7	0.4 ± 0.7	1.3 ± 0.5	0.7 ± 0.5	0.8 ± 0.4	0.5 ± 0.8
Incidence	3/5	3/6	2/7	6/6	4/6	6/6	2/6

Scale: 1, minimal, 2, mild, 3, moderate, 4, marked, 5, severe.

Other studies have shown that CeO_2 induces inflammatory cytokine production in BAL and from isolated alveolar macrophages following IT (Ma et al., 2011) and inhalation (Srinivas et al., 2011) exposures. None of our nanoparticle samples induced the pro-inflammatory cytokines TNF-α, IL-6, or IL-1β over the 84-day time course, despite significant pulmonary PMN and macrophage influx (Figure 5). The lack of significant cytokine production compared to control BAL levels is likely due to differences in collection procedures, as cytokines from this study were measured directly from cell-free BAL rather than from the media of lipopolysaccharide-stimulated BAL cells (Ma et al., 2011). Additionally, differences in dose and exposure route may also account for a lack of inflammatory cytokine signaling measured in this study compared to previous *in vivo* CeO_2 studies (Srinivas et al., 2011). Further, it has been proposed that low cytotoxicity particles must cause excessive lung burden to induce pulmonary inflammation (Oberdorster, 1995); thus, at doses of 1 mg/kg and 0.5 mg/kg, particle-overload may not have occurred or reached sufficient concentrations to induce inflammation as measured by cytokine production.

Ma et al. (2011) demonstrated that CeO_2 nanoparticles severely alter AM responsiveness to zymosan stimulation at 1-day post-exposure; however, this response is diminished by 84-day post-exposure. Our data showed similar results, with BAL cells responding strongly to zymosan stimulation at 1-day post-exposure but minimally 84 days after exposure. Interestingly, our EPR results showed that BAL cells were the most responsive to Cr (VI) stimulation 7-day post-exposure to CeO_2 nanoparticles. This may be due to a shift in the phagocytic cell population from mainly PMNs to a mixture of PMNs and macrophages 7-day post-exposure (Figure 2), a trend that agrees with other nanoparticle exposure studies (Ma et al., 2011; Roursgaard et al., 2011). Interestingly, by 84-day post-exposure, CeO_2 20% Gd BAL cells were significantly hindered in their ability to respond to Cr (VI) compared to BAL cells from control rats. This may be due to a shift in phenotypic characteristics of the macrophage population in the lung from day 1 to day 84. A study by Ma et al. (2011) described an M1 to M2 macrophage population shift following IT CeO_2 exposures, while an *in vitro* silica nanoparticle exposure study showed a similar trend (Hoppstädter et al., 2015). Therefore, changes in macrophage population and phenotype, from residential macrophages originally exposed to CeO_2 nanoparticles to proliferating and recruited macrophages, may account for the altered responsiveness to stimulus by 84-day post-exposure. A potential shift in macrophage populations from M2 cells, which are important in debris clearance, to M1 cells, which are involved in wound healing and anti-inflammatory effects (Rey-Giraud et al., 2012), may also account for the decreased pulmonary damage observed (measured by LDH) over the 84-day time course. Additionally, CeO_2 has been shown to transport throughout the body following IT instillation in rats (Nalabotu et al., 2011; Xiao et al., 2010). However, the lack of pathological changes measured in both liver and kidney sections indicates that by 84-day post-exposure, translocation at toxic, measurable levels had not occurred.

Previous studies have shown that following CeO_2 inhalation in CD1 mice, significant changes in LPO and glutathione levels occur (Aalapati et al., 2014). Therefore, we assessed LPO as a downstream endpoint of oxidative stress. However, in our study, none of the nanoparticles induced significant oxidative lung injury in lung tissue as measured by LPO formation (Figure 4). This is further supported by the lack of free radical production measured by EPR in the absence of Cr (VI) as a stimulus. These differences may be due to the exposure route, dose, and *in vivo* model system variances among studies.

Previous studies have suggested that the valence state of Ce within CeO_2 affects the potential toxicity of the nanoparticles (Colon et al., 2010; Das et al., 2007); however, our findings do not indicate a direct correlation between valence state and toxicity over an 84-day time course. This may be due to low doses that would more closely model human exposure levels and minimal differences in valence state between the CeO_2 10% Gd and CeO_2 20% Gd. Differences in the extent of toxicity between the two doped nanoparticles indicate that the transitional ability of CeO_2, which is hindered by Gd doping, determines its reactivity, rather than valence state ratio. Therefore, further studies are necessary to determine the mechanisms by which doping CeO_2 causes less toxicity initially and yet potentially induces persistent changes overtime. Further, numerous studies have reported that CeO_2 has protective effects *in vitro* and *in vivo* against induced ROS damage (Hashem et al., 2015; Rubio et al., 2015; Zhang et al., 2014), and therefore an *in vivo* study in which damage is induced prior to CeO_2 exposure may allow for the elucidation of differences in reactivity between doped and pure nanoparticles.

Conclusions

The present study aimed to determine the importance of valence state in CeO_2 nanoparticle toxicity following IT exposure in rats by altering the 3+/4+ valence state ratio and increasing oxygen vacancies through doping. While doping the nanoparticles with Gd significantly altered the valence state, minimal differences in pulmonary toxicity were noted between groups. Differences were observed by 84-day post-exposure to pure CeO_2 compounds; specifically that CeO_2 20% Gd significantly increased LDH levels and induced persistent BAL cellular changes compared to PBS controls. This indicates that specific valence state (3+ vs. 4+) may be less important in CeO_2 toxicity than hypothesized and that the ability of CeO_2 to transition between valence states may be more important in determining nanoparticle reactivity. Overall, the toxicity of CeO_2 nanoparticles at low doses following IT in rats was minimal by 84 days. Future studies need to be conducted to determine the effect of valence state on toxicity at higher CeO_2 concentrations and longer post-exposure periods.

Acknowledgements

The authors would like to thank Carrie Long and Dr. Nikki Marshall for insightful conversation about the project. Additionally, the authors would like to thank the histopathology research group at NIOSH for their assistance with tissue fixation and preparation and Shannon Case for her assistance with histopathology methods.

Declaration of interest

The authors report no conflict of interest. The findings and conclusions in this report are those of the authors and do not necessarily represent the views of the National Institute for Occupational Safety and Health.

This project was funded by CDC/NIOSH/HELD Direct funding project (CAN 3927ZJUD). K.M.D. acknowledges support from the National Science Foundation through the IGERT program under grant number, DGE-1144676.

References

Aalapati S, Ganapathy S, Manapuram S, Anumolu G, Prakya BM. 2014. Toxicity and bio-accumulation of inhaled cerium oxide nanoparticles in CD1 mice. Nanotoxicology 8:786–98.

Cassee FR, Van Balen EC, Singh C, Green D, Muijser H, Weinstein J, Dreher K. 2011. Exposure, health and ecological effects review of engineered nanoscale cerium and cerium oxide associated with its use as a fuel additive. Crit Rev Toxicol 41:213–29.

Celardo I, De Nicola M, Mandoli C, Pedersen JZ, Traversa E, Ghibelli L. 2011. Ce^{3+} ions determine redox-dependent anti-apoptotic effect of cerium oxide nanoparticles. ACS Nano 5:4537–49.

Colon J, Hsieh N, Ferguson A, Kupelian P, Seal S, Jenkins DW, Baker CH. 2010. Cerium oxide nanoparticles protect gastrointestinal epithelium from radiation-induced damage by reduction of reactive oxygen species and upregulation of superoxide dismutase 2. Nanomed Nanotechnol 6:698–705.

Das M, Patil S, Bhargava N, Kang JF, Riedel LM, Seal S, Hickman JJ. 2007. Auto-catalytic ceria nanoparticles offer neuroprotection to adult rat spinal cord neurons. Biomaterials 28:1918–25.

Demokritou P, Gass S, Pyrgiotakis G, Cohen JM, Goldsmith W, Mckinney W, et al. 2013. An in vivo and in vitro toxicological characterisation of realistic nanoscale CeO_2 inhalation exposures. Nanotoxicology 7:1338–50.

Dunnick K, Pillai R, Pisane K, Stefaniak A, Sabolsky E, Leonard S. 2015. The effect of cerium oxide nanoparticle valence state on reactive oxygen species and toxicity. Biol Trace Elem Res 166:96–107.

Eom HJ, Choi J. 2009. Oxidative stress of CeO_2 nanoparticles via p38-Nrf-2 signaling pathway in human bronchial epithelial cell, BEAS-2B. Toxicol Lett 187:77–83.

Gantner BN, Simmons RM, Canavera SJ, Akira S, Underhill DM. 2003. Collaborative induction of inflammatory responses by dectin-1 and Toll-like receptor 2. J Exp Med 197:1107–17.

Hashem RM, Rashd LA, Hashem KS, Soliman HM. 2015. Cerium oxide nanoparticles alleviate oxidative stress and decreases Nrf-2/HO-1 in D-GALN/LPS induced hepatotoxicity. Biomed Pharmacother 73:80–6.

Hoppstädter J, Seif M, Dembek A, Cavelius C, Huwer H, Kraegeloh A, Kiemer AK. 2015. M2 polarization enhances silica nanoparticle uptake by macrophages. Front Pharmacol 6:55.

Lin W, Huang YW, Zhou XD, Ma Y. 2006. Toxicity of ceriumoxide nanoparticles in human lung cancer cells. Int J Toxicol 25:451–7.

Ma J, Mercer RR, Barger M, Schwegler-Berry D, Cohen JM, Demokritou P, Castranova V. 2015. Effects of amorphous silica coating on cerium oxide nanoparticles induced pulmonary responses. Toxicol Appl Pharmacol 288:63–73.

Ma JY, Mercer RR, Barger M, Schwegler-Berry D, Scabilloni J, Ma JK, Castranova V. 2012. Induction of pulmonary fibrosis by cerium oxide nanoparticles. Toxicol Appl Pharmacol 262:255–64.

Ma JY, Zhao H, Mercer RR, Barger M, Rao M, Meighan T, et al. 2011. Cerium oxide nanoparticle-induced pulmonary inflammation and alveolar macrophage functional change in rats. Nanotoxicology 5:312–25.

Nalabotu SK, Kolli MB, Triest WE, Ma JY, Manne ND, Katta A, et al. 2011. Intratracheal instillation of cerium oxide nanoparticles induces hepatic toxicity in male Sprague-Dawley rats. Int J Nanomedicine 6:2327–35.

Oberdorster G. 1995. Lung particle overload: implications for occupational exposures to particles. Regul Toxicol Pharmacol 21:123–35.

Pairon JC, Roos F, Sébastien P, Chamak B, Abd-Alsamad I, Bernaudin JF, et al. 1995. Biopersistence of cerium in the human respiratory tract and ultrastructural findings. Am J Ind Med 27:349–58.

Pairon J, Roos F, Iwatsubo Y, Janson X, Billon-Galland M, Bignon J, Brochard P. 1994. Lung retention of cerium in humans. Occup Environ Med 51:195–9.

Park EJ, Choi J, Park YK, Park K. 2008. Oxidative stress induced by cerium oxide nanoparticles in cultured BEAS-2B cells. Toxicology 245:90–100.

Peng L, He X, Zhang P, Zhang J, Li Y, Zhang J, et al. 2014. Comparative pulmonary toxicity of two ceria nanoparticles with the same primary size. Int J Mol Sci 15:6072–85.

Rey-Giraud F, Hafner M, Ries CH. 2012. In vitro generation of monocyte-derived macrophages under serum-free conditions improves their tumor promoting functions. PLoS One 7:e42656.

Riddick T. 1968. Control of Colloid Stability through Zeta Potential: With a Closing Chapter on Its Relationship to Cardiovascular Disease. New York: Livingston.

Roursgaard M, Jensen KA, Poulsen SS, Jensen NEV, Poulsen LK, Hammer M, et al. 2011. Acute and subchronic airway inflammation after intratracheal instillation of quartz and titanium dioxide agglomerates in mice. ScientificWorldJournal 11:801–25.

Rubio L, Annangi B, Vila L, Hernández A, Marcos R. 2015. Antioxidant and anti-genotoxic properties of cerium oxide nanoparticles in a pulmonary-like cell system. Arch Toxicol 90:269–78.

Srinivas A, Rao PJ, Selvam G, Murthy PB, Reddy PN. 2011. Acute inhalation toxicity of cerium oxide nanoparticles in rats. Toxicol Lett 205:105–15.

Vocaturo G, Colombo F, Zanoni M, Rodi F, Sabbioni E, Pietra R. 1983. Human exposure to heavy metals. Rare earth pneumoconiosis in occupational workers. Chest 83:780–3.

Wang Z, Wang Q, Liao Y, Shen G, Gong X, Han N, et al.2011. Comparative study of CeO_2 and doped CeO_2 with tailored oxygen vacancies for CO oxidation. Chemphyschem 12:2763–70.

Xia T, Kovochich M, Liong M, MäDler L, Gilbert B, Shi H, et al. 2008. Comparison of the mechanism of toxicity of zinc oxide and cerium oxide nanoparticles based on dissolution and oxidative stress properties. ACS Nano 2:2121–34.

Xiao H, Haifeng Z, Yuhui M, Wei B, Zhiyong Z, Kai L, et al. 2010. Lung deposition and extrapulmonary translocation of nano-ceria after intratracheal instillation. Nanotechnology 21:285103.

Yoneda S, Emi N, Fujita Y, Ohmichi M, Hirano S, Suzuki KT. 1995. Effects of gadolinium chloride on the rat lung following intratracheal instillation. Fund Appl Toxicol 28:65–70.

Zhang Q, Ge K, Duan J, Chen S, Zhang R, Zhang C, et al. 2014. Cerium oxide nanoparticles protect primary mouse bone marrow stromal cells from apoptosis induced by oxidative stress. J Nanopart Res 16:1–12.

Supplementary material available online

Supplementary Figure 1